Towards surface mapping using GNSS-IR

Corentin Lubeigt[1], François Vincent[2]
[1] *Météo-France, Toulouse, France*
[2] *ISAE-SUPAERO, University of Toulouse, Toulouse, France*

***Abstract*—For more than three decades Global Navigation Satellite Systems (GNSS) were not only seen as a way to obtain a precise position but also as a way to extract geophysical information thanks to reflected signals from surfaces surrounding the receiver as in GNSS Reflectometry (GNSS-R). One of the main GNSS-R techniques, GNSS Interferometric Reflectometry (GNSS-IR), consists of collecting a direct signal and its reflection with a receiver close to the ground. Both signals coherently interfere at the antenna level which results in an interference pattern that can be interpreted in order to extract receiver height or soil moisture for instance. So far, the underlying assumptions for this technique were to consider a flat infinite and homogeneous reflecting surface which contradicts with the ability to map a surface that would need to be non-homogeneous. In this study, an improvement of the signal model is proposed to take into account variations of the reflection coefficient along the surface. This work is limited to a 1D configuration. Closed-form expressions are derived to invert the problem based on the EXtended Invariance Principle (EXIP). Finally, numerical results illustrate this approach.**

***Index Terms*—GNSS-R, signal of opportunity, surface mapping, EXIP.**

I. Introduction

Global Navigation Satellite Systems (GNSS) were originally designed to obtain precise position, velocity and time solutions anywhere on Earth [1], [2]. Soon after the first GNSS constellation was operational, in the early 1990s, unwanted reflected GNSS signals were observed in complex environments such as urban canyon or when the receiver was close to a reflecting surface like sea surface. These reflections, or multipaths, are in general seen as nuisance but they also contain information about the reflecting surface position and nature (roughness, reflectivity). The study of reflected GNSS signals as signals of opportunity in order to extract additional geophysical information is known as GNSS Reflectometry (GNSS-R) and has been a field of research for the last three decades [3], [4].

Among the possible ways to perform GNSS-R, ground-based GNSS Interferometric Reflectometry (GNSS-IR) [5] became a solution of choice, due to its simplicity. In this case, the GNSS receiver is close to the ground so that the direct and reflected signals coherently interfere. As a consequence, it is possible to observe received power variations that can be linked to the height of the receiver and the reflecting coefficient of the surrounding soil. In particular, this is used for tides monitoring [6], soil moisture retrieval [5], [7] or snow depth estimation [8].

In all these GNSS-IR applications where the surface is considered flat, there is a strong assumption: the reflection is commonly modeled as specular such that the reflected energy comes from an ellipse that corresponds to the intersection between the first Fresnel zone and the reflecting surface [9]. The underlying assumption for this model is that the reflecting surface is both homogeneous (reflecting coefficient is the same everywhere) and infinite which makes the surface behaving like a mirror. This contradicts with the will of mapping the reflecting surface with different reflection coefficients as in [10] where the estimated reflection coefficient is associated to an elliptical area for a satellite at a given elevation.

As suggested in [11], a receiver not only collects energy from a surface around the specular point but also from regions farther away. In fact, every point around the receiver is illuminated by the GNSS signal and re-transmits in all directions so that all these contributors must be taken into account to map a non-homogeneous surface.

In this work, the signal model is first improved to tackle the problem of surface mapping based on GNSS-IR. More precisely, the contribution of all elements on the ground is considered to derive the signal model. To estimate the ground reflections, this model has to be inverted. Nevertheless, no closed-form derivation exists. Thereby, the EXtended Invariance Principle (EXIP) [12] is used to derive a closed-form solution which is asymptotically close to the Maximum Likelihood (ML).

The paper is divided as follows: Sec. II presents the signal model along with a discussion on the achievable ground resolution of this approach. In Sec. III, a closed-form solution for the problem at hand is derived. Sec. IV presents numerical results to illustrates the proposed approach. Finally, Sec. V concludes this work and gives some insights for future works.

II. Signal model

A. Considered geometry

The problem at hand is a typical ground-based GNSS-R scenario. A receiver R is placed at a height h above the ground. It receives from a transmitting GNSS satellite T_l placed at an elevation E_l the direct signal with a time-delay τ_l and its reflections from the ground with their corresponding excess delays. The local receiver elevation from the reflecting point placed in y_k is denoted ϕ_k as presented in Fig. 1.

As stated in Sec. I, when considering a uniform reflecting area, the contribution of the ground can be modeled as a

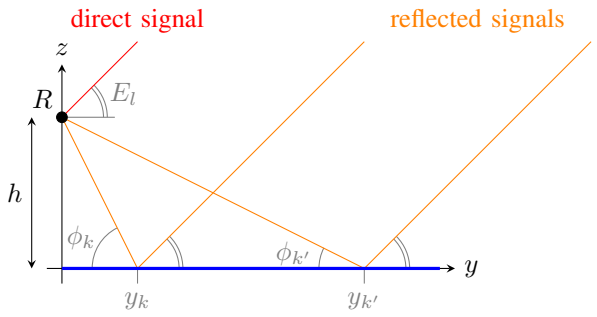

Fig. 1. Problem geometry with a single transmitting satellite.

specular reflection coming from an area defined by the first Fresnel zone [9], [11], [13]. Nevertheless, this assumption is not valid when one wants to map the ground, and each point of the illuminated surface has to be taken into account with its own complex reflection coefficient α. As a consequence, the receiver R collects the sum of all the contributors from the reflecting surface. The additional path Δd for these ground points compared to the direct path can be written as (see Appendix A):

$$\Delta d(\phi_k, E_l) = h\left(\sin(E_l) + \frac{1-\cos(\phi_k)\cos(E_l)}{\sin(\phi_k)}\right). \quad (1)$$

Therefore, for each transmitting satellite in view, the GNSS receiver collects multiple band-limited signal $s_l(t)$, time-delayed and attenuated by the reflections:

$$x(t) = \sum_{l=1}^{L} x_l(t) + w_x(t), \quad (2)$$

where L is the number of satellites seen, $w_x(t)$ is an additive zero-mean complex Gaussian noise and

$$x_l(t) = \beta_l s_l(t-\tau_l) + \beta_l \sum_{k=1}^{K} \alpha_k s_l\left(t - \tau_l - \frac{\Delta d(\phi_k, E_l(t))}{c}\right). \quad (3)$$

A standard GNSS receiver takes the signal $x(t)$ and cross-correlates it with a local replica for an integration time T_I in order to estimate the time-delay τ_l. Assuming that the excess path length $\Delta d(\phi, E_l(t))$ is very small compared to the width of the auto-correlation function resolution, the complex amplitude of the cross-correlation for satellite l can be stacked in a vector as follows:

$$y_l(nT_I) = \beta_l\left(1 + \sum_{k=1}^{K} \alpha_k e^{-j\frac{2\pi}{\lambda}\Delta d(\phi_k, E_l(nT_I))}\right) + w(nT_I), \quad (4)$$

with $n \in (1, N)$, N is the number of post-correlation observations, β_l the amplitude of the direct signal and $w(nT_I)$ is an additive zero-mean complex Gaussian noise with variance σ_n^2.

Equation (4) can be written under a linear matrix expression as follows:

$$\mathbf{y}_l = \beta_l \mathbf{M}_l \boldsymbol{\alpha} + \mathbf{w}, \quad (5)$$

where, for $n \in (1, N)$, $\mathbf{y}_l = (\ldots, y_l(nT_I), \ldots)^T$, $\mathbf{w} = (\ldots, w(nT_I), \ldots)^T$, $\mathbf{M}_l = [\mathbf{1}_N, \mathbf{m}_l(\phi_1), \ldots, \mathbf{m}_l(\phi_K)]$ with $\mathbf{m}_l(\phi_k) = (\ldots, \exp(-j\frac{2\pi}{\lambda}\Delta d(\phi_k, E_l(nT_I)), \ldots)^T$ and $\mathbf{1}_N$ is an N-element column of ones, and $\boldsymbol{\alpha} = (1, \alpha_1, \ldots, \alpha_K)^T$ being the ground reflection mapping to be estimated.

B. Discussion about the resolution

In equation (5), the matrix $\mathbf{M}_l$ is built as a function of the time for the rows and of the local elevation ϕ_k for the columns. In order to simplify the problem, it is of interest to mesh the reflecting surface in terms of ϕ_k so that the columns $\mathbf{m}_l(\phi_k)$ of $\mathbf{M}_l$ are orthogonal with one another, that is, for k and k' both in $(1, K)$

$$\mathbf{m}_l(\phi_k)^H \mathbf{m}_l(\phi_{k'}) = N\delta_{k,k'} \quad (6)$$

It is shown in Appendix B that the condition in equation (6) leads to the following rule to define ϕ_k:

$$\delta\phi \approx \frac{\lambda \sin(\phi)^2}{h\Delta\cos(E_l)}. \quad (7)$$

where $\delta\phi$ is the interval between ϕ_k and ϕ_{k+1} and $\Delta\cos(E_l) = \cos(E_l(NT_I)) - \cos(E_l(T_I))$.

Alternately, instead of meshing following the local receiver elevation ϕ_k, one can mesh following the distance to the receiver $y_k = \frac{h}{tan(\phi_k)}$. Therefore, the range resolution, namely δy is shown to be:

$$\delta y \approx \frac{\lambda}{\Delta\cos(E_l)}. \quad (8)$$

Unlike the Fresnel zone mode, this result suggests that the ground resolution one can get i) does not depend on the receiver height h nor on the considered ground position y_k and ii) is reduced to the wavelength number λ when the observed elevations $E_l(t)$ vary from the horizon to the zenith. Hence a simple regularly meshed wavelength-apart range grid can be used.

In the following, the rule (8) will be adopted to build $\mathbf{M}_l$. In this case, $\mathbf{M}_l^H\mathbf{M}_l \approx N\mathbf{I}_{K+1}$ where $\mathbf{I}_{K+1}$ is the $K+1$-by-$K+1$ identity matrix.

III. Ground Mapping

In order to estimate the ground reflection coefficients vector $\boldsymbol{\alpha}$ in equation (5), the EXIP introduced in [12] is used. This technique consists of i) reparameterization of the current formulation in order to get a simpler solution and ii) refinement of this solution using a weighted least squares (WLS).

A. Reparameterization

Let one consider the following reparameterization of the problem at hand:

$$\boldsymbol{\gamma}_l = \beta_l \boldsymbol{\alpha}, \tag{9}$$

then the problem is simply, for $l \in (1, L)$,

$$\mathbf{y}_l = \mathbf{M}_l \boldsymbol{\gamma}_l + \mathbf{n}. \tag{10}$$

Under the assumption of white Gaussian noise for $\mathbf{n}$, the ML is shown to be the solution of the following least square problem:

$$\widehat{\boldsymbol{\gamma}}_l = \arg\min \mathcal{L}_l(\boldsymbol{\gamma}_l), \tag{11}$$

where $\mathcal{L}_l(\boldsymbol{\gamma}_l) = ||\mathbf{y}_l - \mathbf{M}_l\boldsymbol{\gamma}_l||^2$. The exact solution of this linear problem is shown to be:

$$\widehat{\boldsymbol{\gamma}}_l = \left(\mathbf{M}_l^H \mathbf{M}_l\right)^{-1} \mathbf{M}_l^H \mathbf{y}_l. \tag{12}$$

Thanks to the reparametrization, these L estimated vectors were obtained by processing each satellite contribution separately.

B. Refinement

Now, the last step of EXIP consists in extracting the initial parameters, namely $\widehat{\boldsymbol{\beta}} = (\widehat{\beta}_1, \ldots, \widehat{\beta}_L)^T$ and $\widehat{\boldsymbol{\alpha}}$ from the estimated $\widehat{\boldsymbol{\gamma}}_l$, using a matched WLS minimization. The solution of this WLS procedure is shown to be asymptotically equivalent to the direct ML estimation. This WLS problem is written as

$$(\widehat{\boldsymbol{\beta}}, \widehat{\boldsymbol{\alpha}}) = \arg\min \sum_{l=1}^{L} \|\widehat{\boldsymbol{\gamma}}_l - \beta_l \boldsymbol{\alpha}\|^2_{\mathbf{Q}_l}, \tag{13}$$

where $\mathbf{Q}_l = \frac{\partial^2 \mathcal{L}_l}{\partial \boldsymbol{\gamma}_l \partial \boldsymbol{\gamma}_l^H} = \mathbf{M}_l^H \mathbf{M}_l$. Here the L different norms defined by Q_l make it difficult to solve the WLS problem but, using the appropriate grid defined at the end of Sec. II, $\mathbf{M}_l^H \mathbf{M}_l \approx N \mathbf{I}_{K+1}$, the problem can be approximated as follows:

$$(\widehat{\boldsymbol{\beta}}, \widehat{\boldsymbol{\alpha}}) \approx \arg\min \sum_{l=1}^{L} \|\widehat{\boldsymbol{\gamma}}_l - \beta_l \boldsymbol{\alpha}\|^2 \tag{14}$$

$$\approx \arg\min \mathrm{Tr}\left[\left(\boldsymbol{\Gamma} - \boldsymbol{\alpha}\boldsymbol{\beta}^H\right)^H \left(\boldsymbol{\Gamma} - \boldsymbol{\alpha}\boldsymbol{\beta}^H\right)\right], \tag{15}$$

where $\boldsymbol{\Gamma} = [\widehat{\boldsymbol{\gamma}}_1, \ldots, \widehat{\boldsymbol{\gamma}}_L]$ and $\mathrm{Tr}[\cdot]$ is the trace operator. The trace above can be expanded in several elements as

$$\begin{aligned} &\mathrm{Tr}\left[\left(\boldsymbol{\Gamma} - \boldsymbol{\alpha}\boldsymbol{\beta}^H\right)^H \left(\boldsymbol{\Gamma} - \boldsymbol{\alpha}\boldsymbol{\beta}^H\right)\right] \\ &\quad = \mathrm{Tr}\left[\boldsymbol{\Gamma}^H\boldsymbol{\Gamma}\right] - \boldsymbol{\alpha}^H\boldsymbol{\Gamma}\boldsymbol{\beta} - \boldsymbol{\beta}^H\boldsymbol{\Gamma}^H\boldsymbol{\alpha} + \boldsymbol{\alpha}^H\boldsymbol{\alpha}\boldsymbol{\beta}^H\boldsymbol{\beta}. \end{aligned} \tag{16}$$

In order to minimize (16), one can derive first with respect to $\boldsymbol{\beta}$ and obtain

$$\widehat{\boldsymbol{\beta}} = \frac{\boldsymbol{\Gamma}^H \widehat{\boldsymbol{\alpha}}}{\widehat{\boldsymbol{\alpha}}^H \widehat{\boldsymbol{\alpha}}}, \tag{17}$$

leading to the following maximization problem to get $\widehat{\boldsymbol{\alpha}}$:

$$\widehat{\boldsymbol{\alpha}} = \arg\max \frac{\boldsymbol{\alpha}^H \boldsymbol{\Gamma}\boldsymbol{\Gamma}^H \boldsymbol{\alpha}}{\boldsymbol{\alpha}^H \boldsymbol{\alpha}}, \tag{18}$$

whose solution is shown to be the eigenvector of $\boldsymbol{\Gamma}\boldsymbol{\Gamma}^H$ associated with the largest eigenvalue, that satisfies $\boldsymbol{\alpha}(1) = 1$.

IV. Numerical results

In order to illustrate the performance of the proposed GNSS-IR mapping procedure, let one consider the following scenario: suppose a receiver R set on a mast at $h = 2$ meters above a flat ground. The ground is divided into three areas with different reflection coefficients α_k, $k \in (1, 3)$ (see Table I).

TABLE I
DEFINITION OF THE REFLECTING SURFACE COEFFICIENTS WITH THEIR LOCATION AS A DISTANCE FROM THE RECEIVER.

α_1	α_2	α_3
0m–18.5m	18.5m–25.5m	25.5m–50m
$0.02\exp(j\,\pi/3)$	0.05	$0.02\exp(j\,3\pi/4)$

These surfaces could be seen, for instance, as a flat ground with different water content (α_1 and α_3) on which there is an object that reflects more than the ground (α_2).

The simulation supposes the reception of three satellite signals after correlation, sampled at 0.1Hz during 1.5 hours. During this time, the three satellites are at the same azimuth and their elevations vary monotonously. These variations are depicted in Fig. 2.

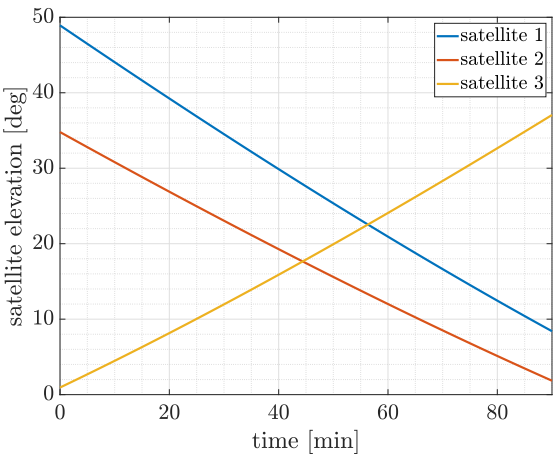

Fig. 2. Satellites elevation during the simulated recording.

Based on these variations and following the discussion in Sec. II-B, one can deduce the grid step to take in order to ensure that $\mathbf{M}_l^H \mathbf{M}_l$ is well conditioned. The smallest $\Delta\cos(E)$ is obtained with satellite 2 ($\Delta\cos(E) \approx 0.178$) which lead to a grid step of 5.6λ. In the following the grid step will be set at $6\lambda \approx 1.2$m.

For the rest of the simulation set-up, the amplitudes for each satellite are set at $\boldsymbol{\beta} = [1500, 1200, 2000]^T$ and the thermal noise standard deviation at $\sigma_n = 200$.

Fig. 3 presents the results of the method described in Sec. III.

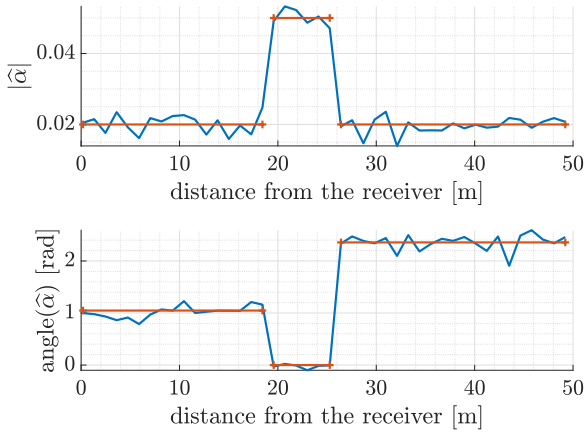

Fig. 3. Estimated $\widehat{\alpha}$ (blue) and true value (orange) as a function of the distance to the receiver. (**Top**) is the estimated amplitude and (**Bottom**) is the estimated phase.

In this figure, one can see the reflecting surface between ∼18m and ∼25m in the top figure. Besides, in the bottom figure, the change in phase is also clearly visible.

V. Conclusion

In this work, a procedure to improve the state of the art GNSS-IR mapping scheme is derived. This procedure is based on an improved signal model that extends the standard specular reflection model. Nevertheless, this more complicated problem does not exhibit any simple closed-form solution. To tackle this problem, the EXIP was used to derive an asymptotically equivalent closed-form solution. This solution is shown to outperform the state of the art procedure based on the first Fresnel zone assumption. Nevertheless the mapping algorithm is limited to a 1D assumption. Future work will aim to extend this procedure to 2D mapping, considering real GNSS data.

Appendix

A. Geometric Phase Computation

Based on Fig. 1, let one fix the coordinates of the transmitter $T(y_T, H)$, the receiver $R(0, h)$ and a point of the reflecting surface $P(y_P, 0)$. The distance between each point can be approximated as follows: $|TP| \approx \sqrt{y_T^2 + H^2} - \frac{h\cos(E)}{\tan(\phi)}$, $|PR| = \frac{h}{\sin(\phi)}$ and $|TR| \approx \sqrt{y_T^2 + H^2} - h\sin(E)$. Therefore, the difference between the reflected path from the poitn P, $|TP| + |PR|$, and the direct path, $|TR|$, is written as:

$$\Delta d(\phi, E) = |TP| + |PR| - |TR| \tag{19}$$

$$\approx h\left(\sin(E) + \frac{1 - \cos(\phi)\cos(E)}{\sin(\phi)}\right). \tag{20}$$

B. Resolution Computation

Let one consider the correlation between two consecutive columns of $\mathbf{M}_l$ separated by an interval $\delta\phi$ as defined in Fig. 4.

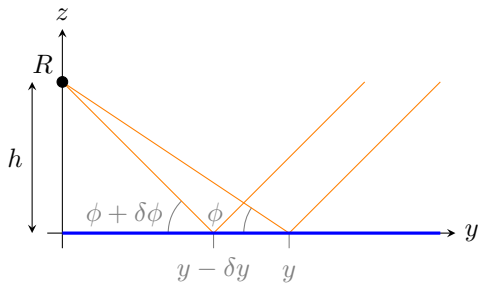

Fig. 4. Variables definition for the resolution computation.

$$\mathbf{m}_l(\phi)^H \mathbf{m}_l(\phi + \delta\phi) = \sum_{n=1}^{N} e^{-j\frac{2\pi}{\lambda}(\Delta d(\phi+\delta\phi, E_{l,n}) - \Delta d(\phi, E_{l,n}))}, \tag{21}$$

where $E_{l,n} = E_l(nT_I)$. Note that for small $\delta\phi$:

$$\Delta d(\phi + \delta\phi, E) = h\left(\sin(E) + \frac{1 - \cos(\phi + \delta\phi)\cos(E)}{\sin(\phi + \delta\phi)}\right) \tag{22}$$

$$\approx \Delta d(\phi + \delta\phi, E) + h\frac{\cos(E) - \cos(\phi)}{\sin(\phi)^2}\delta\phi. \tag{23}$$

Consequently, equation (21) reduces to:

$$\mathbf{m}_l(\phi)^H \mathbf{m}_l(\phi + \delta\phi) \approx \sum_{n=1}^{N} e^{-j\frac{2\pi h\delta\phi}{\lambda}\frac{\cos(E_{l,n}) - \cos(\phi)}{\sin(\phi)^2}}. \tag{24}$$

The idea is to find $\delta\phi$ so that the correlation is null. In other words, assuming that the evolution of the elevation is monotonous, find $\delta\phi$ so that between the beginning ($n = 1$) and the end ($n = N$), the phase in the exponential has turned one period:

$$\frac{h\delta\phi}{\lambda}\frac{\cos(E_{l,N}) - \cos(\phi)}{\sin(\phi)^2} = \frac{h\delta\phi}{\lambda}\frac{\cos(E_{l,1}) - \cos(\phi)}{\sin(\phi)^2} + 1 \tag{25}$$

$$\Leftrightarrow \delta\phi = \frac{\lambda\sin(\phi)^2}{h\Delta\cos(E_l)}. \tag{26}$$

where $\Delta\cos(E_l) = \cos(E_{l,N}) - \cos(E_{l,1})$.

Based on Fig. 4, one can obtain the corresponding interval in terms of distance from the receiver δy:

$$\delta y = \frac{h}{\tan(\phi)} - \frac{h}{\tan(\phi + \delta\phi)} \tag{27}$$

$$\approx \frac{h}{\sin(\phi)^2}\delta\phi = \frac{\lambda}{\Delta\cos(E)}. \tag{28}$$

REFERENCES

[1] E. D. Kaplan and C. J. Hegarty, Eds., *Understanding GPS/GNSS: Principle and Applications*, 3rd ed. Artech House, 2017.

[2] P. J. G. Teunissen and O. Montenbruck, Eds., *Handbook of Global Navigation Satellite Systems*. Springer, 2017.

[3] M. Martín-Neira, "A Passive Reflectometry and Interferometry System (PARIS): Application to Ocean Altimetry," *ESA Journal*, vol. 17, 1993, US Patent 5 546 087, Aug. 13 1996.

[4] V. U. Zavorotny and A. G. Voronovich, "Scattering of GPS Signals from the Ocean with Wind Remote Sensing Application," *IEEE Transactions on Geoscience and Remote Sensing*, vol. 38, no. 2, pp. 951–964, 3 2000.

[5] K. M. Larson, E. E. Small, E. D. Gutmann, A. L. Bilich, J. J. Braun, and V. U. Zavorotny, "Use of GPS Receivers as a Soil Moisture Network for Water Cycle Studies," *Geophysical Research Letters*, vol. 35, no. 24, 2008.

[6] P. Zeiger, F. Frappart, J. Darrozes, N. Roussel, P. Bonneton, N. Bonneton, and G. Detandt, "SNR-Based Water Height Retrieval in Rivers: Application to High Amplitude Asymmetric Tides in the Garonne River," *Remote Sensing*, vol. 13, no. 9, 2021.

[7] V. U. Zavorotny, K. M. Larson, J. J. Braun, E. E. Small, E. D. Gutmann, and A. L. Bilich, "A physical model for GPS multipath caused by land reflections: toward bare soil moisture retrievals," *IEEE Journal of Selected Topics in Applied Earth Observations and Remote Sensing*, vol. 3, no. 1, pp. 100–110, 2010.

[8] M. Durand, A. Rivera, F. Geremia-Nievinski, M. G. Lenzano, J. F. G. Monico, P. Paredes, and L. Lenzano, "GPS Reflectometry Study Detecting Snow Height Changes in the Southern Patagonia Icefield," *Cold Regions Science and Technology*, vol. 166, p. 102840, 2019.

[9] A. Camps and J. F. Munoz-Martin, "Analytical Computation of the Spatial Resolution in GNSS-R and Experimental Validation at L1 and L5," *Remote Sensing*, vol. 12, no. 23, p. 3910, 2020.

[10] N. Rodriguez-Alvarez, A. Camps, M. Vall-Llossera, X. Bosch-Lluis, A. Monerris, I. Ramos-Perez, E. Valencia, J. F. Marchan-Hernandez, J. Martinez-Fernandez, G. Baroncini-Turricchia *et al.*, "Land Geophysical Parameters Retrieval Using the Interference Pattern GNSS-R Technique," *IEEE Transactions on Geoscience and Remote Sensing*, vol. 49, no. 1, pp. 71–84, 2010.

[11] A. Camps, "Spatial Resolution in GNSS-R Under Coherent Scattering," *IEEE Geoscience and Remote Sensing Letters*, vol. 17, no. 1, pp. 32–36, 2020.

[12] P. Stoica and T. Söderström, "On reparametrization of loss functions used in estimation and the invariance principle," *Signal processing*, vol. 17, no. 4, pp. 383–387, 1989.

[13] F. Zimmermann, B. Schmitz, L. Klingbeil, and H. Kuhlmann, "GPS multipath analysis using fresnel zones," *Sensors*, vol. 19, no. 1, p. 25, 2018.